Supplement of Biogeosciences, 22, 41–53, 2025
https://doi.org/10.5194/bg-22-41-2025-supplement


Biogeosciences
Open Access

*Supplement of*

# Molecular-level characterization of supraglacial dissolved and water-extractable organic matter along a hydrological flow path in a Greenland Ice Sheet micro-catchment

**Eva L. Doting et al.**

*Correspondence to:* Eva L. Doting (edoting@sas.upenn.edu)

# S1. Supplementary methods

### S1.1 Hydrology

Hydraulic conductivity and water table height were calculated from recharge curves in five auger holes with an initial radius of 70 mm and depth of 400 – 450 mm. Throughout the duration of the experiment, surface lowering caused an effective reduction in auger hole depth. Recharge rate was recorded using ultrasonic rangefinders at a 1Hz resolution, and recharge curves were processed as described in Stevens et al. (2018). The height of the water table was defined following the completion of recharge, i.e. when water in the auger hole stopped rising. Full recharge holes were emptied using a siphon prior to the subsequent recharge measurement.

Orthoimages and DEMs of the site were created using aerial imagery from a UAV (DJI Mini 2) at 9:00, 14:00, and 21:00 on the sampling day. Flight elevation was 20 m, whilst the camera was set with a fixed aperture (*f*2.8) and ISO (100), with shutter speed and UAV airspeed adjusted to suit the prevailing light conditions. One orthophoto and DEM were constructed per image-set, at a resolution of 0.024 m/pixel using the commercially available Agisoft MetashapePro (Agisoft, Russia) and GNSS-derived position from the UAV (i.e. this was not corrected using ground control points).
Hydrological modelling of the weathering crust was undertaken to establish water flow direction and magnitude, which was used to drive a particle tracking tool to establish hydrological connectivity between auger hole D and the supraglacial stream. The model used was the 'Darcy Velocity' groundwater flow direction and magnitude model included in the Spatial Analyst package of ArcMap 10.8 (esri, USA). This tool requires the following inputs: hydraulic head, effective porosity, saturated thickness and transmissivity (itself a function of the saturated thickness and hydraulic conductivity). As the weathering crust is an unconfined aquifer (e.g. (Müller and Keeler, 1969)), the hydraulic head  is equivalent to the absolute elevation of the water table (Cohen and Cherry, 2020). The water table (and therefore hydraulic head) was interpolated across the study area using the 'Topo-to-Raster' tool, tied with manually digitized streams and point measurements of absolute water table from each borehole (i.e., DEM elevation minus water depth from the surface). Effective porosity was parameterized as 0.35, assuming a saturated ice density of 550 kg $m^{-3}$ (after (Cooper et al., 2018)). Saturated thickness was calculated using the interpolated water table, and a parameterized weathering crust depth of 50 cm from the surface (Irvine-Fynn et al., 2021; Stevens et al., 2018), and is multiplied by median hydraulic conductivity for each time window, derived from point measurements, to establish transmissivity. Note that there is no hydraulic conductivity measurement at site A at 14:00 and 21:00, and these values are parameterized using available data from this hole and consideration of temporal hydraulic conductivity trends in holes B-E. The modelled flow vector field was used to drive the 'Particle Track' tool for auger hole D, producing modelled flow path of water from this hole.

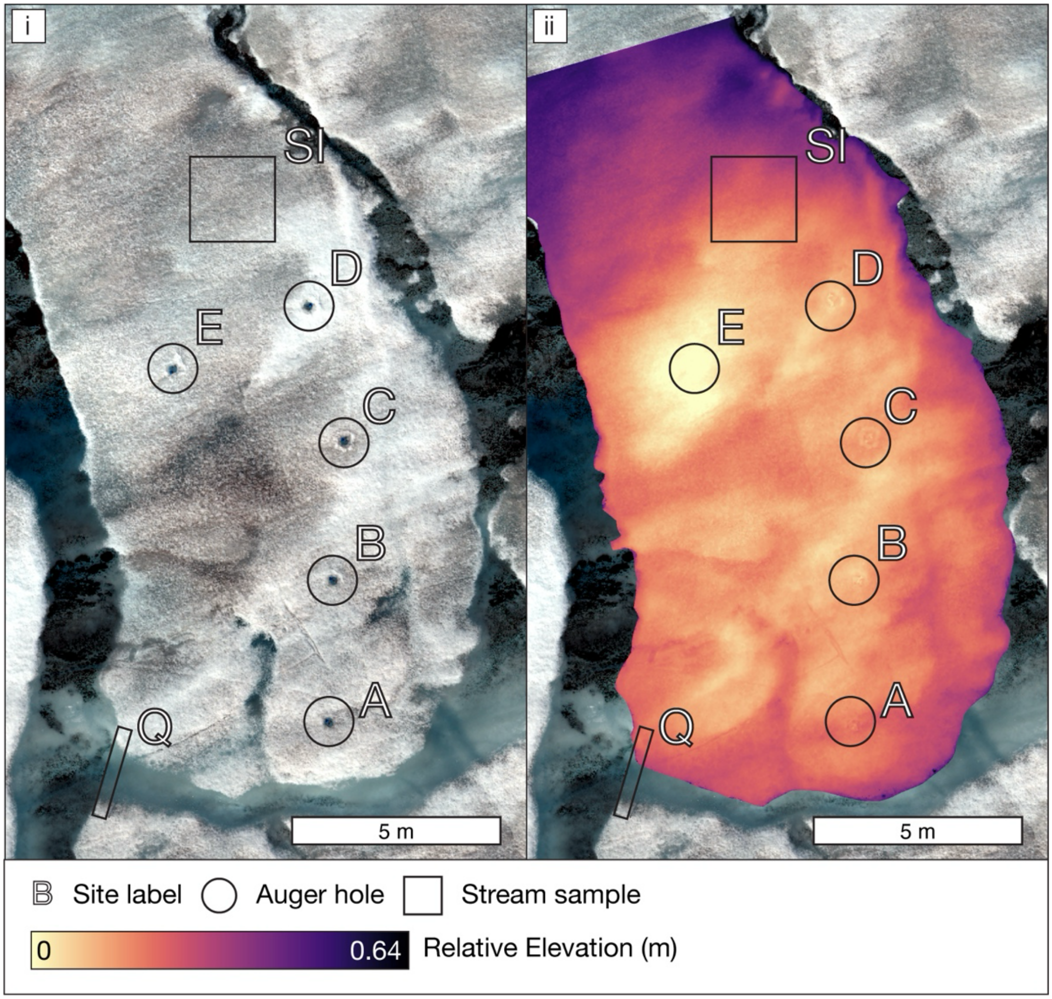


**Figure S1 | A DSM (panel ii) of the study site, with sampling locations marked. Note that elevations are relative to a reference datum, not mean sea level. The orthophoto provided in Fig 1 is included for reference (panel i).**

### S1.2 FT-ICR MS instrumentation and acquisition settings

Sample solution was infused via a micro-electrospray source (Emmett et al., 1998) (50 µm i.d. fused silica emitter) at 500 nL/min by a syringe pump. Typical conditions for negative ion formation were: emitter voltage, -2.4-2.9 kV; tube lens, –250 V; and heated metal capillary current, 7 A. DOM extracts were analysed with a custom-built hybrid linear ion trap FT-ICR mass spectrometer equipped with a 21 T superconducting solenoid magnet (Hendrickson et al., 2015; Smith et al., 2018). Ions were initially accumulated in an external multipole ion guide (1-5 ms) and released *m/z*-dependently by decrease of an auxiliary radio frequency potential between the multipole rods and the end-cap electrode (Kaiser et al., 2013). Ions were excited to *m/z*-dependent radius to maximize the dynamic range and number of observed mass spectral peaks (32-64%), and excitation and detection were performed on the same pair of electrodes (Chen et al., 2014). The dynamically harmonized ICR cell in the 21 T FT-ICR is operated with 6 V trapping potential (Boldin and Nikolaev, 2011; Kaiser et al., 2013). Time-domain transients of 3.1 seconds were acquired with the Predator data station that handled excitation and detection only, initiated by a TTL trigger from the commercial Thermo data station, with 100 time-domain acquisitions averaged for all experiments (Blakney et al., 2011). Mass spectra were phase-corrected (Xian et al., 2010) and internally calibrated with 10-15 highly abundant homologous series that span the entire molecular weight distribution based on the "walking" calibration method (Savory et al., 2011). Experimentally measured masses were converted from the International Union of pure and Applied Chemistry (IUPAC) mass scale to the Kendrick mass scale (Kendrick, 1963) for rapid identification of homologous series for each heteroatom class (i.e. species with the same $C_CH_HN_NO_OS_S$ content, differing only by the degree of alkylation) (Hughey et al., 2001).

**Table S1 The number of formulae assigned per FT-ICR MS file, prior to blank correction, and the RMS error per assigned file. All calibrated peak lists and assigned files, and a list of all elemental compositons assigned across the dataset, are publicly available via the Open Science Framework (https://osf.io/) via DOI 10.17605/OSF.IO/JRBTH.**

| File name in OSF | Sample group | Number assigned formulae | RMS error |
|---|---|---|---|
| X2021December02_weathering_crust_R1_sum100_assigned.csv.RelAbun | Weathering crust | 11,537 | 0.054 |
| X2021December02_weathering_crust_R2_sum100_assigned.csv.RelAbun | Weathering crust | 13,761 | 0.054 |
| X2021December02_weathering_crust_R3_sum100_assigned.csv.RelAbun | Weathering crust | 12,756 | 0.055 |
| X2021December02_weathering_crust_R4_sum100_assigned.csv.RelAbun | Weathering crust | 11,930 | 0.046 |
| X2021December02_field_blank_sum100_assigned.csv.RelAbun | Procedural blank | 4,365 | 0.100 |
| X2021December02_supraglacial_stream_R1_sum100_assigned.csv.RelAbun | Supraglacial stream | 13,347 | 0.050 |
| X2021December02_supraglacial_stream_R2_sum100_assigned.csv.RelAbun | Supraglacial stream | 12,307 | 0.068 |
| X2021December02_supraglacial_stream_R3_sum100_assigned.csv.RelAbun | Supraglacial stream | 12,634 | 0.050 |
| X2021December02_supraglacial_stream_R4_sum100_assigned.csv.RelAbun | Supraglacial stream | 9,774 | 0.054 |
| X2021December02_supraglacial_stream_R5_sum100_assigned.csv.RelAbun | Supraglacial stream | 10,096 | 0.056 |
| X2021December02_dark_ice_R1_sum100_assigned.csv.RelAbun | Surface ice | 11,155 | 0.050 |
| X2021December02_dark_ice_R2_sum100_assigned.csv.RelAbun | Surface ice | 8,684 | 0.067 |
| X2021December02_dark_ice_R3_sum100_assigned.csv.RelAbun | Surface ice | 9,763 | 0.052 |
| X2021December02_dark_ice_R4_sum100_assigned.csv.RelAbun | Surface ice | 11,710 | 0.056 |
| X2022January26_laboratory_leachate_R1_sum100_assigned.csv.RelAbun | SIP-WEOM | 6,617 | 0.078 |
| X2022January26_laboratory_leachate_R2_sum100_assigned.csv.RelAbun | SIP-WEOM | 8,340 | 0.099 |
| X2022January26_laboratory_leachate_R3_sum100_assigned.csv.RelAbun | SIP-WEOM | 6,514 | 0.056 |
| X2022January26_laboratory_leachate_R4_sum100_assigned.csv.RelAbun | SIP-WEOM | 7,543 | 0.064 |

**Table S2 Principal Component Analysis Structure Matrix of DOM parameters**

| Parameter | PC1 | PC2 |
|---|---|---|
| Formulae (#) | -0.462 | 0.059 |
| $Mass^{wa}$ (Da) | 0.553 | 0.796 |
| $NOSC^{wa}$ | 1.026 | 0.102 |
| $AI_{mod}^{wa}$ | 1.021 | -0.081 |
| Aliphatic High O/C (%RA) | -0.624 | 0.754 |
| Aliphatic Low O/C (%RA) | -0.903 | -0.499 |
| HUP High O/C (%RA) | 1.008 | 0.012 |
| HUP Low O/C (%RA) | -0.525 | 0.863 |
| Peptide-like (%RA) | -0.896 | 0.170 |
| Condensed aromatic (%RA) | 0.993 | -0.144 |
| Polyphenolic (%RA) | 0.990 | -0.174 |
| CHO (%RA) | 0.797 | 0.640 |
| CHON (%RA) | -0.686 | 0.755 |
| CHOS (%RA) | -0.609 | -0.821 |

## References


Blakney, G. T., Hendrickson, C. L., and Marshall, A. G.: Predator data station: A fast data acquisition system for advanced FT-ICR MS experiments, Int. J. Mass Spectrom., 306, 246–252, https://doi.org/10.1016/j.ijms.2011.03.009, 2011.

Boldin, I. A. and Nikolaev, E. N.: Fourier transform ion cyclotron resonance cell with dynamic harmonization of the electric field in the whole volume by shaping of the excitation and detection electrode assembly, Rapid Commun. Mass Spectrom., 25, 122–126, https://doi.org/10.1002/rcm.4838, 2011.

Chen, T., Beu, S. C., Kaiser, N. K., and Hendrickson, C. L.: Note: Optimized circuit for excitation and detection with one pair of electrodes for improved Fourier transform ion cyclotron resonance mass spectrometry, Rev. Sci. Instrum., 85, 2012–2015, https://doi.org/10.1063/1.4883179, 2014.

Cohen, A. J. B. and Cherry, J. A.: Conceptual and Visual Understanding of Hydraulic Head and Groundwater Flow, 58 pp., 2020.

Cooper, M. G., Smith, L. C., Rennermalm, A. K., Mige, C., Pitcher, L. H., Ryan, J. C., Yang, K., and Cooley, S. W.: Meltwater storage in low-density near-surface bare ice in the Greenland ice sheet ablation zone, Cryosphere, 12, 955–970, https://doi.org/10.5194/TC-12-955-2018, 2018.

Emmett, M. R., White, F. M., Hendrickson, C. L., Shi, D. H., and Marshall, A. G.: Application of micro-electrospray liquid chromatography techniques to FT-ICR MS to enable high-sensitivity biological analysis, J. Am. Soc. Mass Spectrom., 9, 333–340, https://doi.org/10.1016/S1044-0305(97)00287-0, 1998.

Hendrickson, C. L., Quinn, J. P., Kaiser, N. K., Smith, D. F., Blakney, G. T., Chen, T., Marshall, A. G., Weisbrod, C. R., and Beu, S. C.: 21 Tesla Fourier Transform Ion Cyclotron Resonance Mass Spectrometer: A National Resource for Ultrahigh Resolution Mass Analysis, J. Am. Soc. Mass Spectrom., 26, 1626–1632, https://doi.org/10.1007/s13361-015-1182-2, 2015.

Hughey, C. A., Hendrickson, C. L., Rodgers, R. P., Marshall, A. G., and Qian, K.: Kendrick mass defect spectrum: A compact visual analysis for ultrahigh-resolution broadband mass spectra, Anal. Chem., 73, 4676–4681, https://doi.org/10.1021/ac010560w, 2001.

Irvine-Fynn, T. D. L., Edwards, A., Stevens, I. T., Mitchell, A. C., Bunting, P., Box, J. E., Cameron, K. A., Cook, J. M., Naegeli, K., Rassner, S. M. E., Ryan, J. C., Stibal, M., Williamson, C. J., and Hubbard, A.: Storage and export of microbial biomass across the western Greenland Ice Sheet, Nat. Commun. 2021 121, 12, 1–11, https://doi.org/10.1038/s41467-021-24040-9, 2021.

Kaiser, N. K., McKenna, A. M., Savory, J. J., Hendrickson, C. L., and Marshall, A. G.: Tailored ion radius distribution for increased dynamic range in FT-ICR mass analysis of complex mixtures, Anal. Chem., 85, 265–272, https://doi.org/10.1021/ac302678v, 2013.

Kendrick, E.: A mass scale based resolution mass spectrometry of organic compounds, Anal. Chem., 35, 2146–2154, 1963.

Müller, F. and Keeler, C. M.: Errors in Short-Term Ablation Measurements on Melting Ice Surfaces, J. Glaciol., 8, 91–105, https://doi.org/10.3189/S0022143000020785, 1969.

Savory, J. J., Kaiser, N. K., Mckenna, A. M., Xian, F., Blakney, G. T., Rodgers, R. P., Hendrickson, C. L., and Marshall, A. G.: Measurement Accuracy with a “Walking” Calibration Equation, Anal. Chem., 83, 1732–1736, 2011.

Smith, D. F., Podgorski, D. C., Rodgers, R. P., Blakney, G. T., and Hendrickson, C. L.: 21 Tesla FT-ICR Mass Spectrometer for Ultrahigh-Resolution Analysis of Complex Organic Mixtures, Anal. Chem., 90, 2041–2047, https://doi.org/10.1021/ACS.ANALCHEM.7B04159/ASSET/IMAGES/MEDIUM/AC-2017-04159Q_0010.GIF, 2018.

Stevens, I. T., Irvine-Fynn, T. D. L., Porter, P. R., Cook, J. M., Edwards, A., Smart, M., Moorman, B. J., Hodson, A. J., and Mitchell, A. C.: Near-surface hydraulic conductivity of northern hemisphere glaciers, Hydrol. Process., 32, 850–865, https://doi.org/10.1002/HYP.11439, 2018.

Xian, F., Hendrickson, C. L., Blakney, G. T., Beu, S. C., and Marshall, A. G.: Automated broadband phase correction of fourier transform ion cyclotron resonance mass spectra, Anal. Chem., 82, 8807–8812, https://doi.org/10.1021/ac101091w, 2010.